

Fluorescence antibunching microscopy

O. Schwartz¹ and D. Oron¹

¹*Department of Physics of Complex Systems, Weizmann Institute of Science, Rehovot, Israel*

Breaking the diffraction limit in microscopy by utilizing quantum properties of light has been the goal of intense research in the recent years. We propose a quantum superresolution technique based on non-classical emission statistics of fluorescent markers, routinely used as contrast labels for bio-imaging. The technique can be readily implemented using standard fluorescence microscopy equipment.

Increasing the imaging resolution in optical microscopy can potentially benefit many fields of research, including life sciences. In classical linear optics, diffraction imposes a limit on the resolution of far-field microscopy. In the last two decades, a number of techniques have been developed that break this limit by making use of non-linear optical processes[1–3]. The diffraction limit can also be effectively overcome by utilizing contrast labels exhibiting strong variations in brightness, either induced by photoactivation[4–6] or intrinsic [7, 8], in effect allowing for localization of individual fluorophores while the rest are dark.

Quantum optics offers another promising pathway to superresolution imaging. Quantum optical methods have been shown to dramatically increase the resolution in interferometric measurements[9], and allowed for imaging sensitivity enhancement beyond shot noise[10]. At the same time, superresolution via quantum imaging has not yet been demonstrated experimentally. The theoretical research aiming at achieving sub-diffraction limited quantum imaging has mainly focused on the scenario wherein an absorptive object is illuminated with a non-classical light beam. Superresolution is then attained via two main routes. One requires an object consisting of or stained with a multi-photon absorbing material. In this scheme, the diffraction limit is overcome by utilizing the high spatial frequency quantum interference patterns, similarly to quantum superresolution lithography[11]. Although multi-photon interference patterns of high order have been observed experimentally using coincidence detection[12, 13], the lack of a low light level multi-photon absorber makes this approach currently not feasible. The other pathway to achieving sub-diffraction resolution is probing an object with a beam of light exhibiting position (or momentum) entanglement. The high resolution images can then be obtained simply by coincidence detection[14, 15]. Although momentum entangled light can be produced by spontaneous parametric down conversion[16, 17], the resolution in this case is limited by the diffraction limit at the pumping wavelength. Increasing the resolution further requires a bright highly entangled light source, which is yet to be developed.

The above superresolution schemes exploit quantum properties of the illuminating light and thus require non-

classical light sources. The alternative is, to image an object naturally emitting non-classical light, such as cascaded emission from a three-level system [18] or resonant fluorescence[19]. The multi-photon interference patterns observable in the far field can be used for superresolved imaging of the emitters. While this approach can be feasible for imaging trapped ions, its reliance on fragile quantum effects makes it impractical for bio-imaging conditions.

In this paper, we consider a different property of fluorescence emitters: photon antibunching[20], arising from the tendency of fluorophores to emit photons one by one rather than in bursts. Antibunching is a distinctively quantum phenomenon, implying reduced quantum fluctuations (squeezing) of light[21] and sub-Poissonian photon statistics[22]. On the other hand, it is a very robust effect, exhibited by various fluorophores at room temperature[23–25]. We study the non-classical photon statistics of fluorescence in connection to fluorescence microscopy and show that it can be used for superresolved microscopic imaging under realistic conditions.

For simplicity, we focus on the case of pulsed excitation, with the pulse duration much shorter, and the interval between pulses much longer than the fluorescence lifetime. Upon excitation, a single fluorophore emits at most one photon, with a probability p . Such behavior is profoundly different from the Poissonian statistics of classical light. In particular, the variance of the number of fluorescent photons emitted in a series of M excitation cycles is $V = Mp(1 - p)$, while the mean photon number is $\langle N \rangle = Mp$. A classical light source with the same photon flux would yield a variance $V_P = \langle N \rangle$. The variance of the fluorescent photon number is thus reduced by a factor of $(1 - p)$ with respect to the classical shot noise.

The nonclassical statistics of fluorescent light can be used to produce superresolved images of fluorophores. Consider a fluorescent emitter, imaged by a microscopic imaging system onto a pixelated (or scanning) detector with a photon number resolving capability. At every detector position x , the probability P to detect a photon emitted by the fluorophore is given by

$$P(x) = pQSh(x - x_0), \quad (1)$$

where Q is the quantum efficiency of the detector, S denotes optical collection efficiency, h is the point spread

function of the imaging system and x_0 describes the coordinates of the fluorophore image. The photon number variance becomes a function of detector position: $V(x) = MP(x)(1 - P(x))$. For a set of several fluorophores, since the emission events in different fluorophores are uncorrelated, the variance of the total photon number is given by the sum of variances (??) for every emitter:

$$V(x) = M \sum_{\alpha} P_{\alpha}(x)(1 - P_{\alpha}(x)) = \quad (2)$$

where p_{α} and x_{α} are the emission probability and the image position of the fluorophore α .

The difference between eq.(2) and the classical shot noise variance at the same mean flux quantifies the degree of antibunching of fluorescent light and can therefore be called the antibunching signal:

$$A(x) \equiv V(x) - \langle N(x) \rangle = -MQ^2S^2 \sum_{\alpha} p_{\alpha}^2 h^2(x - x_{\alpha}). \quad (3)$$

This signal corresponds to an effective point spread function $h_A(x) = h^2(x)$. In Fourier domain, h_A spans the interval of frequencies twice as large as that of h . The antibunching microscopy thus enables imaging with up to double resolution, similarly to the resolution improvement attainable with 2-photon microscopy.

The mechanism of the antibunching microscopy is illustrated in Fig. 1 for the case of two identical emitters. The emitters are not resolved in the fluorescent signal, while two separate peaks are visible in the antibunching signal.

It is instructive to consider photon statistics in the limit of small photon flux. Let $F_1(x)$ and $F_2(x)$ be the probabilities of detecting exactly one and two photons, respectively, at a given detector position. In terms of these probabilities, the average photon number and the variance become $\langle N \rangle = M(F_1(x) + 2F_2(x))$ and $V(x) = M(F_1 + 4F_2 - F_1^2)$. The antibunching signal (3) then takes the form of $A(x) = M(2F_2(x) - F_1^2(x))$. Since this expression vanishes for Poissonian statistics, the antibunching signal can be regarded as a measure of the lack of two photon coincidence events with respect to classical light.

This observation elucidates the mechanism of the resolution increase shown in Fig. 1: in this example, a coincidence event involves detection of one photon from each of the fluorophores. The probability of a coincidence event therefore has a sharp maximum positioned between the two emitters. This is in contrast to the case of two classical emitters, for which a pair of photons could as well originate from a single emitter, making the maximum less sharp.

The antibunching signal (3) is determined by the optical signal autocorrelation at a given detector position. Fluorescence antibunching is also manifest in the cross

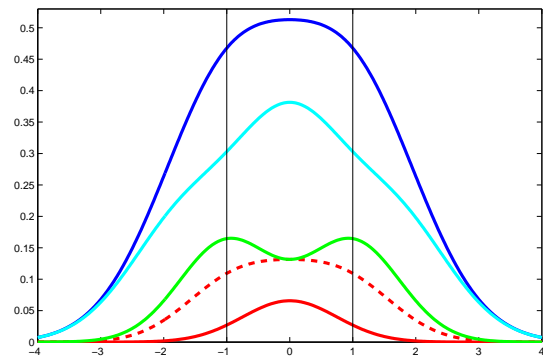


FIG. 1: Antibunching imaging of two fluorescent emitters. The vertical lines denote the locations of two fluorescent emitters. The blue line is the regular fluorescent signal, the cyan line represents the variance given by eq.(2), the green line is the antibunching signal (3). The solid red line shows the probability F_2 of a two-photon coincidence event with a sharp peak in the center. The dashed red line shows the same probability for two classical emitters, featuring a wider peak. The plots are calculated for $P_1 = P_2 = 0.4$, with a gaussian point spread function with an RMS width of $\sigma = 1.06$.

correlation between the photon numbers N_1, N_2 detected in a pair of proximate detectors. Similarly to variance, the covariance of the two signals $V^{\times}(x_1, x_2) = \langle N_1 N_2 \rangle - \langle N_1 \rangle \langle N_2 \rangle$ is a sum of individual fluorophore contributions. For classical light, the signals observed in the detectors are uncorrelated and therefore covariance vanishes. In contrast, an individual fluorophore produces only one photon at a time, which can be detected in only one of the detectors, leading to $N_1 N_2 = 0$. The covariance antibunching signal can thus be defined as:

$$A^{\times}(x_1, x_2) = \sum V_{\alpha}^{\times}(x_1, x_2) = -M \sum P_{\alpha}^{(1)} P_{\alpha}^{(2)} \quad (4)$$

where x_1, x_2 are the detector positions, $P_{\alpha}^{(1)}$ and $P_{\alpha}^{(2)}$ are the detection probabilities for a given fluorophore at the two detectors. The antibunching signal (4) contains a product of two optical point spread functions. As we show below, it can be used to produce higher resolution images along with the autocorrelation antibunching signal (3).

We numerically tested the resolution improvement in antibunching microscopy by performing a Monte Carlo simulation of the antibunching imaging process using a pixelated detector array. For efficient signal utilization, we used both the autocorrelation antibunching signal of Eq. (3) and the cross correlation data (4) to form the image. The autocorrelation antibunching signal at a given pixel, numbered by a two-dimensional index j , is given by

$$A_j = \sum_{\alpha} (p_{\alpha}^j)^2 = V_j - \langle N_j \rangle, \quad (5)$$

where $\langle N_j \rangle$ is the mean number of photons, and V_j is the variance of the photon number. The cross correlation contribution to the second order antibunching signal was calculated as a weighted sum of the cross correlations of the pairs of pixels $j \pm \delta$, centered at the pixel j . The simulation was carried out as follows: a stack of frames was generated; in each frame, for every fluorophore it was decided at random whether it emits a photon (with a probability $p = 0.5$). If a photon was emitted, it was randomly positioned with a probability density corresponding to a Gaussian point spread function. The resulting stack of frames was used to compute the second order antibunching signal according to the following formula:

$$A_j = \sum_{\delta} W(\delta) \left(\langle N_{j+\delta} N_{j-\delta} \rangle - \langle N_{j+\delta} \rangle \langle N_{j-\delta} \rangle \right) - \langle N_j \rangle, \quad (6)$$

where N_j is the number of photons detected in the pixel j , δ is a summation index labeling the pixel pairs, $W(\delta)$ is the weight assigned to the pixel pairs ($W(0) = 1$), and the angular brackets denote averaging over the set of frames. The above analysis does not fully utilize the cross-correlation information: indeed, only a half of all pixel pairs are centered in a certain pixel. A pair of, for example, two adjacent pixels has its center between the two pixels. It is therefore possible to compute the antibunching signal in ‘virtual pixels’ in between adjacent pixels, i.e. with at least one of the two components of j being half-integer[26]. The effective number of pixels in each direction is thus doubled, increasing the total amount of pixels by a factor of four. The signal in the ‘virtual’ pixels was calculated using Eq. (6), with the last term omitted and with one or both components of the summation index δ assuming half-integer values (so that $i \pm \delta$ are integer). The results of the simulation shown in Fig. 2 demonstrate a significant improvement of resolution: the individual emitters, which cannot be discerned by regular imaging, are clearly resolved in the antibunching image.

The antibunching signal, defined above in terms of second order momenta, serves as a measure of the lack of two-photon coincidence events, hence it can be called the second order antibunching signal. The n -th order antibunching signal $A_n(x)$, quantifying the lack of n -photon events, can be defined in terms of the irreducible parts of the n -th order momenta known as cumulants[27]. The defining property of cumulants is that they are additive for independent random variables, which allows one to express the cumulants of the observed signal as a sum of the individual fluorophore contributions. For a single fluorophore, the n -th order cumulant is given by $C_n = MP(1-P) \dots (1-(n-1)P)$. The cumulants $C_n(x)$ of the total signal are therefore given by

$$C_n(x) = M \sum_{\alpha} P_{\alpha}(x) (1 - P_{\alpha}(x)) \dots (1 - (n-1)P_{\alpha}(x)). \quad (7)$$

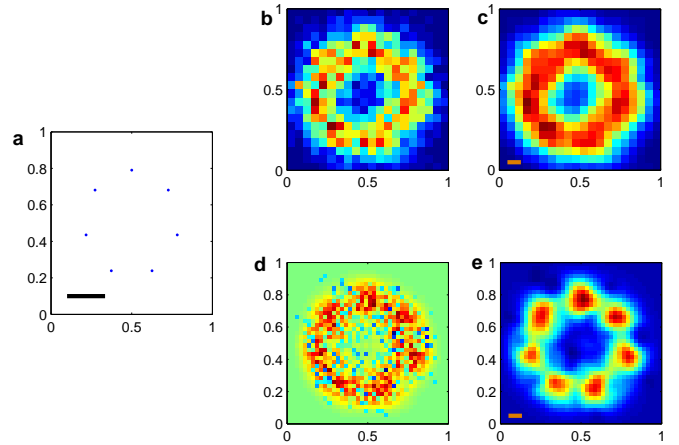


FIG. 2: A simulation of the second order antibunching imaging: resolving individual emitters. **(a)**: seven emitters are arranged in a ring. The scalebar shows full width at half maximum (FWHM) of the optical point spread function. **(b)**: Regular imaging shows a ring structure, but the individual emitters are not resolved. **(c)**: the same image as in (b), smoothed by a Gaussian filter to reduce the noise (filter FWHM is shown by the scalebar). **(d)**: the second order antibunching image. **(e)** the same image smoothed using the same filter as in (c). The individual emitters are clearly discerned. The image was formed from 1000 frames.

The antibunching signal of order n can then be defined as

$$A_n = M \sum P_{\alpha}^n, \quad (8)$$

which can be expressed via cumulants of order $k \leq n$ using Eq. (7):

$$A_n(x) = M \sum_k (\hat{R}^n)_{1k} C_k(x), \quad (9)$$

where $(\hat{R}^n)_{1k}$ is the first row of the n -th power of a matrix \hat{R} , all elements of which are zero except

$$R_{kk} = -R_{k-1k} = 1/k. \quad (10)$$

The signals $A_n(x)$ vanish in the classical limit, and are therefore a valid local measure of the degree of antibunching. For $n = 2$ the above expressions yield the second order antibunching signal described above. Substituting eq. (1) into the definition (8) one obtains

$$A_n(x) = MQ^n S^n \sum_{\alpha} p_{\alpha}^n [h(x - x_i)]^n. \quad (11)$$

Effectively, the n -th order antibunching signal corresponds to a point spread function $h_m(x) = [h(x)]^m$. Similarly to the second order, this enables imaging with resolution up to n times better than diffraction limited in three dimensions[2, 28].

Quantum fluorescence imaging requires fluorophores with as high quantum yield as possible. Fortunately, many of the fluorescent markers widely used in bio-imaging, such as organic dyes, have a quantum yield approaching unity. Very high quantum yield has also been demonstrated with colloidal semiconductor quantum dots[29].

Many fluorescent single photon emitters exhibit random variations of brightness known as blinking. Blinking increases the observed photon number fluctuations, and could be expected to change the photon statistics to super-Poissonian. It turns out, however, not to be the case: indeed, for a single emitter, the photon number follows a Bernoulli distribution even in the presence of blinking, the only consequence of which is an effective reduction of the emission probability. As long as blinking of individual fluorophores is uncorrelated, the antibunching properties of emission statistics persist for an arbitrary number of emitters.

The photon number distributions required for computing the cumulants in Eq. (9) can be determined with a scanning number resolving detector[30, 31]. Another option is using a regular or an electron multiplying charged coupled device (ccd)[15]. An electron multiplying ccd in the photon counting regime can be used as a pixelated number resolving detector, provided that the number of pixels sufficiently large so that the probability of detecting more than one photon in a pixel is small. Interestingly, a regular ccd, which is naturally a photon number resolving detector, can also be used despite significant amount of noise in the output. Since the noise is statistically independent from the number of photons, it can be removed from the signal by subtracting the pre-measured cumulants of the noise from the observed cumulants.

The antibunching microscopy can be regarded as a quantum version of superresolution optical fluctuation imaging (SOFI)[7]: in this technique, the n -th order signal is given by n -th cumulant, without the lower order ‘correction’ terms appearing in Eq. (9). Interestingly, the antibunching signal vanishes in the classical limit, instead of turning into the corresponding SOFI expression. This is the case because the two schemes exploit different sources of non-Poissonian statistics: while SOFI quantifies the super-Poissonian brightness fluctuations of essentially classical sources, in the present scheme the signal is due to the reduction of the quantum fluctuations with respect to the classical shot noise. The antibunching signal is thus generated by steadily emitting fluorophores, which enables continuous superresolved monitoring of the samples stained with fluorescent markers.

In conclusion, we propose a fluorescence microscopy imaging modality that allows for sub-diffraction-limited imaging by virtue of quantum properties of fluorescence

emission. Despite being ostensibly quantum, the technique does not require a non-classical light source and does not depend on fragile quantum interference effects. The proposed method can be implemented with current technology, or indeed with a regular fluorescence microscope.

-
- [1] K. Fujita et al., Phys. Rev. Lett. **99**, 228105 (2007).
 - [2] M. G. L. Gustafsson, Proc. Nat. Acad. Sci. **102**, 13081 (2005).
 - [3] S. Hell and J. Wichmann, Optics Letters **19**, 780 (1994).
 - [4] E. Betzig et al., Science **313**, 1642 (2006).
 - [5] S. Hess, T. Girirajan, and M. Mason, Biophysical journal **91**, 4258 (2006).
 - [6] M. B. Michael J. Rust and X. Zhuang, Nature Methods **3**, 793 (2006).
 - [7] T. Dertinger et al., Proc. Nat. Acad. Sci. **106**, 22287 (2009).
 - [8] K. Lidke et al., Optics Express **13**, 7052 (2005).
 - [9] V. Giovannetti, S. Lloyd, and L. Maccone, Science **306**, 1330 (2004).
 - [10] G. Brida, M. Genovese, and I. Berchera, Nature Photonics **4**, 227 (2010).
 - [11] M. D’Angelo, M. V. Chekhova, and Y. Shih, Phys. Rev. Lett. **87**, 013602 (2001).
 - [12] I. Afek, O. Ambar, and Y. Silberberg, Science **328**, 879 (2010).
 - [13] P. Walther et al., Nature **429**, 158 (2004).
 - [14] V. Giovannetti et al., Physical Review A **79**, 13827 (2009).
 - [15] M. Tsang, Phys. Rev. Lett. **102**, 253601 (2009).
 - [16] E. Fonseca, C. Monken, and S. Pádua, Phys. Rev. Lett. **82**, 2868 (1999).
 - [17] W. A. T. Nogueira et al., Phys. Rev. Lett. **86**, 4009 (2001).
 - [18] A. Muthukrishnan, M. Scully, and M. Zubairy, Journal of Optics B **6**, S575 (2004).
 - [19] C. Thiel et al., Phys. Rev. Lett. **99**, 133603 (2007).
 - [20] H. Kimble, M. Dagenais, and L. Mandel, Phys. Rev. Lett. **39**, 691 (1977).
 - [21] D. F. Walls and P. Zoller, Phys. Rev. Lett. **47**, 709 (1981).
 - [22] L. Mandel, Opt. Lett. **4**, 205 (1979).
 - [23] R. Brouri et al., Opt. Lett. **25**, 1294 (2000).
 - [24] B. Lounis et al., Chem. Phys. Lett. **329**, 399 (2000).
 - [25] W. Patrick Ambrose et al., Chem. Phys. Lett. **269**, 365 (1997).
 - [26] T. Dertinger et al., Opt. Exp. **18**, 18875 (2010).
 - [27] M. Kendall and A. Stuart, *The advanced theory of statistics. Vol.1: Distribution theory* (1977).
 - [28] O. Schwartz and D. Oron, Opt. Lett. **34**, 464 (2009).
 - [29] Y. Chen et al., J. Am. Chem. Soc. **130**, 5026 (2008).
 - [30] F. Guerrieri et al., Phys. Rev. Lett. **105**, 163602 (2010).
 - [31] A. Lita, A. Miller, and S. Nam, Opt. Exp. **16**, 3032 (2008).